Electronic Raman scattering in the 2D antiferromagnet NiPS₃

Xingzhi Wang^{1*}, Jun Cao¹, Hua Li², Zhengguang Lu^{3,4}, Arielle Cohen⁵, Anubhab Haldar⁵, Hikari Kitadai¹, Qishuo Tan¹, Kenneth S. Burch⁶, Dmitry Smirnov³, Weigao Xu², Sahar Sharifzadeh^{1,5,7,8}, Liangbo Liang⁹, Xi Ling^{1,5,10*}

¹ Department of Chemistry, Boston University, Boston, Massachusetts 02215, USA.

² Key Laboratory of Mesoscopic Chemistry, School of Chemistry and Chemical Engineering, Nanjing University, Nanjing 210023, China.

³ National High Magnetic Field Laboratory, Tallahassee, Florida 32310, USA.

⁴ Department of Physics, Florida State University, Tallahassee, Florida 32306, USA.

⁵ Division of Materials Science and Engineering, Boston University, Boston, Massachusetts 02215, USA.

⁶ Department of Physics, Boston College, Chestnut Hill, Massachusetts 02467, USA.

⁷ Department of Electrical and Computer Engineering, Boston University, Boston, Massachusetts 02215, USA.

⁸ Department of Physics, Boston University, Boston, Massachusetts 02215, USA.

⁹ Center for Nanophase Materials Sciences, Oak Ridge National Laboratory, Oak Ridge, Tennessee 37831, United States

¹⁰ The Photonics Center, Boston University, Boston, Massachusetts 02215, USA.

^{*}To whom the correspondence should be addressed. Email address: xzwang@bu.edu; xiling@bu.edu

Abstract

Correlated-electron systems have long been an important platform for various interesting phenomena and fundamental problems in condensed matter physics. As a pivotal process in this system, d-d transition has been suggested as the key towards the achievement of optical spin-control in van der Waals magnets. However, it is still unclear that how the d-d excitations behave in a quasi-2D system with strong electronic correlation and spin-charge coupling. Here we present a systematic investigation on the d-d transition in van der Waals antiferromagnets - NiPS₃ from bulk to atomically thin flakes via electronic Raman spectroscopy. Two electronic Raman modes with large Raman shift at ~ 1.0 eV are observed under a wide range of excitations from 454 to 531 nm. Such light scattering originates from the coupling between the incident photons and d electrons in Ni²⁺ ions, resulting an intra-atom d-d transition between $^3A_{2g}$ and $^3T_{2g}$ states. This electronic process persists down to at least tri-layer flakes, and exhibits an insensitivity to the spin ordering in the materials in the magneto-optical study. Our study demonstrates the power of electronic Raman scattering in investigating the unique electronic structure and its coupling to magnetism in atomically thin correlated 2D magnets.

Introduction

Van der Waals (vdW) magnetic materials have received growing interest revealing new physics in the extreme nanoscale limit (1-5). Recently, attentions have been focused on a new antiferromagnet, nickel phosphorus trisulfides (NiPS₃), due to its intriguing physics in quasi two-dimensional (2D) systems, including phonon-magnon coupling (6), strong electron correlation (7) and spin-correlated excitonic physics (8-10). As a 2D magnet with strongly correlated d electrons, d-d transition in NiPS₃ plays an important role in determining and controlling spin properties (11, 12). For example, light-induced magnetic anisotropy has been demonstrated in $NiPS_3$ by optically pumping the d electrons to the higher-energy orbital states of Ni²⁺ ions (11). Despite extensive interest in low-dimensional correlated systems, it is striking that few studies have focused on d-d excitations in atomically thin vdW layers (13-15). The d-d excitations in 2D layers are expected to be different from that in the bulk cases, because the onsite coulomb repulsion (Hubbard U) can be modified by the increasing dielectric screening (16). However, due to the forbidden selection rule, the absorptions corresponding to the d-d transitions in NiPS₃ are much weaker compared to the inter-band transitions, and generally become undetectable in the absorption spectra of the thin layers (7). Such invisibility prevents the ability to uncover the subtle changes in the correlated d electron states in 2D systems.

Raman spectroscopy has been an effective optical tool with non-destructivity and high sensitivity in the study of elemental excitations, including phonons, excitons, polaritons, magnons, and spinons in condensed matter systems (17-19). The selection rule of Raman scattering offers great capabilities to reveal the symmetry and coupling to magnetism in various 2D magnets (20-24). Electronic Raman (ER) scattering, where photons are scattered by electronic excitations in the materials, has be utilized in revealing the electronic behaviors in low-dimensional materials, such as metallic carbon nanotubes and AlGaAs epilayers (25, 26). NiPS₃ exhibits a unique electronic structure with a highly localized electronic band composed by d orbitals (9, 27), suggesting a potential to explore the d-d transitions in 2D systems by ER spectroscopy.

In this letter, we report the observation of ER scattering in NiPS₃ layers for the first time and present a systematic study on the origin and correlation with the spin structure.

Two ER modes with energies around 1.0 eV have been observed far below the band gap under a wide range of excitation from 454 to 531 nm in NiPS₃ down to few-layer flakes. Such ER scattering is attributed to the photon scattering by the *d-d* excitations, which represent electronic transition between *d* orbitals in Ni²⁺ ions. In contrast to the spin-correlated inter-band transitions, *d-d* transitions exhibit distinct independence on the formation of spin-structure near Néel temperature (T_N) and on external magnetic field. Our study suggests the ER scattering to be a unique probe to reveal the electronic transitions related to *d* orbitals in 2D strong-correlated systems, which can provide rich physical information for the study of fundamental physics and the design of ultrathin opto-magneto devices.

Results

NiPS₃ has been of interest for its realization of antiferromagnetic XXZ model on a honeycomb lattice (28, 29). As temperature decreases across its $T_N = \sim 152$ K, NiPS₃ undergoes a magnetic phase transition from the paramagnetic to the antiferromagnetic phase (28). High-quality NiPS₃ single crystals were grown using a chemical vapor transport method (30). Monolayer NiPS₃ crystal has a hexagonal lattice structure with three-fold rotation symmetry, which is broken by the monoclinic interlayer stacking order in few-layer and bulk cases (see Fig. 1A and Fig. S1A). When the temperature is below its T_N , the spins form a zigzag antiferromagnetic order, where the intra-layer spin moments are arranged ferromagnetically in chains, but are coupled antiferromagnetically with their neighboring chains (see Fig. S1B). The planes are also coupled ferromagnetically along the c direction. The spin direction in NiPS₃ is mainly along the c-axis, with an angle of c-8° out of the c-ab-plane (c-29).

Fig. 1B displays a typical optical spectrum from an exfoliated thick NiPS₃ flake (~50 nm) under a 458-nm laser excitation at 295 K. The spectrum shows three peaks, ranging from the visible to the near infrared region. However, distinct spectra are obtained as the excitation wavelength varies from 454 nm (2.73 eV) to 531 nm (2.34 eV) (see Fig. 1C). A peak located at ~ 1.39 eV is observed in all spectra under different laser excitations. The origin of this peak is attributed to the photoluminescence (PL) from the band edge transition, in consideration of its energy position near the reported optical absorption edge

at ~ 1.5 eV (9, 10). In contrast, the other two peaks, labeled as R₁ and R₂, exhibit an obvious redshift with the decrease of the excitation energy, and finally disappear when the excitation energy is below ~ 2.35 eV. More importantly, each of the two peaks presents a fixed energy difference between the collected signal and the laser excitation, suggesting that their origin is Raman scattering rather than luminescence (see Fig. 2A).

Typically, Raman peaks in insulating magnets result from either phonons or magnons (6, 31). However, these two types of excitations can be excluded as the origin of R₁ and R₂ in NiPS₃ based on multiple pieces of evidence. First, the Raman shifts of these two peaks are ~ 0.93 and 1.05 eV, which are much higher than the frequencies of phonon or magnon modes (6, 32). Second, the observed Raman peaks have larger peak width of over 0.1 eV, in contrast to the narrow feature of one-phonon or one-magnon modes (33, 34). In addition, the temperature and polarization dependent studies, which will be discussed in detail later, indicate that the behaviors of these two peaks are different from the two-magnon mode, which has been observed at $400 \sim 600 \text{ cm}^{-1}$ in NiPS₃ (6). In contrast to the phonon and magnon modes, the large Raman shifts of the two peaks imply that they originate from electronic transitions. To confirm this, the electronic band structure and density of states for bulk NiPS₃ were calculated using first-principles density functional theory (DFT)+U method with U = 4.0 eV (see Fig. S3) (6, 7, 9). The calculated band structure clearly shows the near-flat electronic bands near the conduction band minimum (CBM), which are predominantly contributed by Ni d orbitals (see Fig. S3C). The small dispersion of these bands is due to the localization of the Ni d orbitals. In contrast, the valence bands are mostly from S p orbitals, leading to dispersive valance bands that are common in many other materials (see Fig. S3D). The calculation indicates an indirect band gap ~ 1.6 eV, which is consistent with the previous calculation and experimental absorption edge (7, 27, 30).

In order to reveal the origin of the two Raman peaks (i.e. R_1 and R_2), the absorbance measurement has been performed on thick NiPS₃ samples (see Fig. 2B). Strong and saturated absorption is observed above ~1.5 eV, which can be attributed to the inter-band transition as predicted by our calculation. Interestingly, a relatively weak absorption feature is observed at ~ 1.0 eV. This absorption far below band gap can be resolved into two

components with energies at ~ 0.92 and ~ 1.09 eV, in a good agreement with the Raman shifts of R₁ and R₂, suggesting that they originate from the same transition in the material. Such absorption was reported to result from d-d transitions on the transition metal ions in NiPS₃, as well as many other transition metal compounds (14, 35-37). The nickel atom is located at the center of a trigonally distorted octahedral crystal field, constituting of six sulfur atoms (see Fig. 2C). As a result, the d orbitals of Ni^{2+} ion split into several states, among which the ground state ${}^{3}A_{2g}$ and the first excited state ${}^{3}T_{2g}$ are directly involved in the observed ER scattering with large Raman shift at ~1.0 eV (see Fig. 2D). Moreover, due to the trigonal distortion, the ${}^3T_{2g}$ state further splits into ${}^3A_{1g}$ and ${}^3E_{g}$ states, leading to the observation of two ER modes that correspond to the transition ${}^{3}A_{2g} \rightarrow {}^{3}A_{1g}$ and ${}^{3}A_{2g} \rightarrow {}^{3}E_{g}$. Note that DFT+U calculation does not reveal these features of d orbitals, instead predicting a charge transfer (s/p to d) transition at 1.45 eV. This discrepancy may be due to the fact that DFT+U may fail for describing certain physical properties of strongly correlated materials. This approach does not fully account for the multi-correlated nature of d orbitals (38, 39); additionally, the lack of self-interaction error correction for s/p states and lack of excitonic effects can result in an error in the predicted nature of transitions (37, 38). Considering the selection rule for angular momentum conservation, direct d-d transitions are generally forbidden, while it becomes allowed due to the vibrionic coupling in materials (13, 40).

The intensity of ER peaks exhibit a clear dependence on the excitation energy, indicating a resonant effect, which is related to an external electronic state as an intermediate state (see Fig. 2E). The ER intensity can be given by the formula as (41, 42),

$$I(E_L) = \frac{A}{|(E_L - E_{mi} - i\Gamma)(E_L - E_{mi} - E_{ex} - i\Gamma)|^2},$$

where A is a constant related to the electron-photon coupling; E_L , E_{mi} , and E_{ex} are the incident photon energy, the intermediate state energy, and excited state energy, respectively; Γ is the damping constant. ER intensity will achieve a maximum when $E_L = E_{mi} + E_{ex}$. The intensities of electronic Raman modes, R_1 and R_2 , reach the maximum at ~ 2.61 and ~ 2.73 eV, respectively. The different resonant energies of two modes indicate a scattered light resonance, where $E_L = E_{mi} + E_{ex}$. Therefore, E_{mi} can be obtained as

~1.70 eV by $E_{mi} = E_L - E_{ex}$, which matches the energy of the second excited state (${}^3T_{1g}$) from the ground state (11, 12).

As a van der Waals antiferromagnet, NiPS₃ exhibits various intriguing properties and offers a unique opportunity to explore strongly correlated electron systems and magnetic systems in the 2D limit. Especially, d-d excitations play an important role in determining electronic and spin properties of NiPS₃ (11). Benefited from the under-band absorption at ~ 1.0 eV, d-d transitions can be detected in bulk NiPS₃. However, with the reduction of the sample thickness, the under-band absorption dramatically decreases and finally becomes undetectable in atomically thin samples, and thus prevents the relative studies in 2D systems. The resonance condition enhances the signal and enables the ER scattering in NiPS₃, resulting the detectable signals of d-d excitations in thin layers for exploring the evolution of the local electronic configuration upon thinning and stacking. As shown in Fig. 3A, the ER spectroscopy study was performed on exfoliated NiPS₃ layers, where the ER modes can be resolved in NiPS₃ from bulk down to tri-layer samples, with the intensity decreasing with the reduction of layer-number. Both ER modes exhibit a blue shift in the thinner samples, i.e., the energies of two d-d excitations increasing with the reduction of layer-number (see Fig. 3B). This phenomenon indicates an increasing of crystal field splitting energy of d orbitals, originating from a stronger octahedral crystal field around Ni²⁺ in atomically thin samples. Furthermore, with less layer number of samples, the energy difference between two ER modes also shows a slight increase, suggesting a larger splitting of ${}^3T_{2g}$ state and trigonal distortion in few-layer samples.

Due to its antiferromagnetic nature, the optical properties of NiPS₃, such as low-frequency Raman modes and optical absorption, have showed correlations to the magnetic structure, and exhibit distinct behaviors with variations of temperature and external field (6, 7). Specifically, it has been demonstrated that the excitonic emission in NiPS₃ is strongly correlated to the spin structure, which gives rise to a distinct linear polarization of the excitonic emission (8-10, 43). However, the correlation between spins and d electrons remains unexplored, especially in low-dimensional structures. To this end, the temperature dependent ER spectroscopy measurements are conducted (see Fig. 3C). As the R₂ mode becomes hard to be resolved at low temperature due to the reduced population of the higher

energy state, the following discussion related to low temperature data mainly focuses on R₁ mode. With the change of temperature from 10 to 300 K, the peak position, integrated intensity and full width at half maximum (FWHM) of R₁ peak exhibit gradual variation, which could be attributed to the lattice contraction with the reduction of temperature (see Fig. S5). In spite of the formation of spin ordering, no dramatic change of the ER modes is observed across T_N. Our result indicates that the ER processes are isolated from the spin structure in NiPS₃, suggesting that the corresponding d-d transitions occur on a single Ni atom. Additionally, it is worth noting that the ER modes have a broad peak width of tens of meV even at 10 K (see Fig. S5A). Such a low temperature generally suppresses the thermal population of energy levels, and results in a narrow feature of optical signals (8, 44). The broad feature of ER modes can be attributed to two reasons. First, d orbitals of Ni²⁺ ions further split into more fine features due to the spin-orbit coupling, leading to a broad ER signal consisting of multiple electronic transitions (11, 41). Second, a strong vibrionic coupling is involved in the d-d transitions which are generally forbidden and requires the assistance of other media, such as phonons. As a result, ER modes are broadened due to the mismatch of nuclear coordinates (see Fig. S5D). To further confirm that the d-d transitions are isolated from the spin effect, the ER study was conducted at 5 K under the external in-plane and out-of-plane magnetic fields (see Fig. 3D and Fig. S6). The results show that ER modes are also insensitive to the applied fields up to 14 T in the Voigt geometry and up to 17 T in the Faraday geometry. Since the in-plane field induced spin-flop transition in NiPS₃ has been found in the magneto-PL study and isothermal magnetization measurement (9, 45), the unchanged ER signal as a function of an applied in-plane field further proves that the d-d excitations are insensitive to the spin ordering in the material.

For potential opto-spintronic applications, the polarization behavior of the d-d excitations would play a significant role. To this end, we performed a systematic polarization-resolved ER measurement on exfoliated NiPS₃ flakes. Both R₁ and R₂ modes exhibit stronger intensities in the parallel configuration (XX) compared to that in the cross configuration (XY) in the linear polarization study (see Fig. S7A). Similarly, in the circular polarization measurement, the two ER peaks also show a stronger intensity in the parallel configuration ($\sigma^+\sigma^-$) (see Fig. S7B).

As a result, both ER modes in NiPS₃ exhibit an A_{1g} symmetry. By calculating the linear polarization degree $(\rho_l = \frac{I_{XX} - I_{XY}}{I_{XX} + I_{XY}})$ and the circular polarization degree $(\rho_c = \frac{I_{\sigma^+ \sigma^+} - I_{\sigma^+ \sigma^-}}{I_{\sigma^+ \sigma^+} + I_{\sigma^+ \sigma^-}})$, R₁ mode exhibits a $\rho_l \sim 49\%$ and a $\rho_c \sim 25\%$ at room temperature (see Fig. S7C). Moreover, we further conducted a polarization angle dependent study on NiPS₃ in two configurations: (I) rotating the polarization of collection light (P_{col}) with fixed polarization of incident light (P_{in}) and (II) rotating P_{in} with fixed P_{col} . Clear two-fold signals emerge in the polar plot of polarization-dependent intensity of two ER modes in two configurations, in agreement with their A_{1g} symmetry (see Fig. 4A and 4B). The intensities of both ER modes can be fitted by $I_{ER} = I_0 + A\cos^2\theta$, where θ is the angle between P_{in} and P_{col} ; I_0 and A are fitting constants. In contrast, in the azimuthal-angle dependent study, where the sample is rotating with fixed $P_{in} \parallel P_{col}$ (Configuration III), ER intensity shows independence on the crystal orientation at room temperature (see Fig. 4C). However, when the temperature goes down to 77 K, NiPS₃ become antiferromagnetic and R₁ mode exhibits an anisotropic response (see Fig. 4C). The intensity of R_1 peak can be fitted by $I_{ER} = I_1 + I_2$ $B \sin^2 \varphi$, where φ is the angle between light polarization and the b axis of the crystal; I_1 and B are fitting constants. We define the linear polarization degree, $\rho = (I_a I_b$)/($I_a + I_b$), where I_a (I_b) is the R₁ intensity when light polarization (both P_{in} and P_{col}) is parallel to the a(b) axis. The linear polarization degree of R_1 can be obtained ~ 5% at 77 K. To confirm the relation between the spin structure and the emerging polarization of R₁ mode, we conduct the temperature-dependent polarized ER measurement. The polarization degree of R_1 mode drops significantly when the temperature approaches to $T_N = 152$ K and finally disappears in the paramagnetic phase (see Fig. 4D). The temperature dependent polarization degree in the antiferromagnetic phase is fitted well by $\rho(T) \sim \left|1 - \frac{T}{T_{N}}\right|^{2\beta}$, where β is a critical exponent indicating the decay trend near the phase transition temperature (46). We obtain $\beta = 0.27 \pm 0.03$, which is in accordance with $\beta = 0.23 \sim 0.26$ for the temperature-dependent magnetic intensity in 2D XY systems (47) and the β for the spin-induced linear polarization degree of sharp emission of NiPS₃ at 1.476 eV (8-10). This agreement suggests that the linear polarization of R₁ mode arises from the anisotropy of spins structure in NiPS₃. Considering the insensitivity of d-d transition to the spin ordering, the anisotropic ER response may be the consequence of the anisotropic absorption of

incident photons due to the magnetic linear dichroism of materials, of which polarization degree is at the same order as ER response (9, 10).

Discussion

As a correlated 2D antiferromagnet, NiPS₃ offers a unique opportunity to explore strongly correlated electron systems and magnetism in the 2D limit. Specifically, the investigation on *d-d* excitation is necessary in revealing various fundamental characters, such as crystal field splitting, local Hund's coupling and Hubbard U, which are crucial for electronic structure and exchange coupling in materials. However, the forbidden selection rule of *d-d* transition raises the difficulty in its direct observation in 2D layers through absorption spectroscopy, thus prevents the fundamental study in strongly correlated electron physics in 2D limits. In this work, the *d-d* excitations are successfully probed on atomically thin NiPS₃ layers by ER spectroscopy. We further conduct a systematic study on *d-d* excitations, which reveals the evolution trend with the reduction of sample thickness and the insensitivity to the spin ordering. Our ER study not only provides new insights in the electronic properties and electron-spin coupling in correlated 2D antiferromagnets NiPS₃, but also demonstrates the power of ER spectroscopy in the investigation of correlated 2D magnets and twisted heterostructures, which could potentially open new pathways to controlling the correlations in Mott systems.

Materials and Methods

Sample preparation. NiPS₃ single crystals were grown using a chemical vapor transport method (30). A stoichiometric amount of high-purity elements (mole ratio Ni:P:S = 1:1:3, around 1 g in total) and iodine (about 10–20 mg) as a transport agent were sealed into a quartz ampule and kept in a two-zone furnace (650–600 °C). The length of the quartz ampule is about 16 cm with a 13 mm external diameter. The pressure inside the ampule was pumped down to 1×10^{-4} Torr. After 1 week of heating, the ampule was cooled down to room temperature with bulk crystals in the lower temperature end. The purity of the synthesized sample has been confirmed by series of characterizations in our previous work

(9). Few-layer NiPS₃ flakes were prepared on Si substrates with 285-nm SiO₂ layers by mechanical exfoliation from a bulk single crystal.

Optical spectroscopy measurements. The ER scattering and PL measurements were carried out on a micro-Raman spectrometer (Horiba-JY T64000) and the signal was collected through a $50\times$ long-working-distance objective. A cryostat (Cryo Industry of America, USA) was used to provide a vacuum environment and a continuous temperature from 5 to 300 K by liquid helium flow. Both ER scattering and PL measurements were perform using a single-grating mode with a 150 g/mm grating in backscattered geometry. A series of laser lines, ranging from 454 to 568 nm, were from a Kr^+/Ar^+ ion laser (Coherent Innova 70C Spectrum) and used to excite the sample. The absorbance measurement was conducted on a spectrophotometer (Agilent Cary 5000). The polarized optical measurements were performed on another micro-Raman spectrometer (Horiba HR Evolution) and the signal was collected through a $100\times$ objective with correction ring. The signals were dispersed with a 100 g/mm grating. A solid-state laser ($\lambda=473$ -nm) was used to excite the sample.

Magneto-PL measurements. The magneto-PL experiments were conducted in the National High Magnetic Field Lab. The magneto-optical experiments were performed on bulk crystal with a 14 T magnet in the Voigt geometry and a 17 T magnet in the Faraday geometry. A 488-nm continuous-wave laser was used to excite the sample. For the measurements in the Voigt geometry, the sample was vertically put inside the magnetic cell with the surface parallel to the applied magnetic field. A mirror was set between objective and sample with 45° to change the optical path by 90°. A 10× objective was used to focus the excitation laser onto the sample and also used to collect the PL signal, which subsequently past through a multi-mode optical fiber and was measured by a spectrometer with a CCD camera (Princeton Instruments, IsoPlane 320).

Theoretical calculations. Spin-polarized density functional theory (DFT) calculations were carried out using the Vienna Ab Initio Simulation Package (VASP) (48). Electronion interactions were described by projector-augmented-wave (PAW) pseudopotentials and exchange-correlation interactions were captured by the generalized gradient approximation (GGA) with the Perdew-Burke-Ernzerhof (PBE) functional (49). To

describe the strong electron correlation effects of localized Ni 3*d* orbitals in NiPS₃, a simplified (rotationally invariant) DFT+U_{eff} approach (50) was adopted with an effective U parameter of 4.0 eV, a common value used in previous studies (6, 7, 9). The DFT-D3 method was used for considering the van der Waals interactions between the layers (51). The lattice constants and atomic positions of bulk NiPS₃ were both relaxed until the residual forces were below 0.01 eV/Å, where the cutoff energy was set at 350 eV and the gamma-centered K-point mesh was 12×6×12. Initial magnetic moments of 4 or -4 were chosen for each Ni atom in the experimental zigzag antiferromagnetic order.

Acknowledgements

This material is based upon work supported by the National Science Foundation (NSF) under Grant No.(1945364). X.W. and X.L. acknowledge the financial support from Boston University. X.L. acknowledges the membership of the Boston University Photonics Center. L.L. acknowledges computational resources of the Compute and Data Environment for Science (CADES) at the Oak Ridge National Laboratory, which is supported by the Office of Science of the U.S. Department of Energy under Contract No. DE-AC05-00OR22725. A portion of this research (DFT calculations) used resources at the Center for Nanophase Materials Sciences, which is a U.S. Department of Energy Office of Science User Facility. A.C. and S.S. acknowledge financial support from the U.S. Department of Energy (DOE), Office of Science, Basic Energy Sciences (BES) Early Career Program under Award No. DESC0018080. The authors acknowledge the computational resources through the Extreme Science and Engineering Discovery Environment (XSEDE), which is supported by National Science Foundation grant number ACI-1548562; and the National Energy Research Scientific Computing Center, a DOE Office of Science User Facility supported by the Office of Science of the U.S. Department of Energy under Contract No. DE-AC02-05CH11231. W.X. acknowledges the National Natural Science Foundation of China (21873048), the Natural Science Foundation of Jiangsu Province (BK20180319). Z.L. and D.S. acknowledge support from the US Department of Energy (no. DE-FG02-07ER46451) for high-field magnetospectroscopy measurements performed at National High Magnetic Field Laboratory, which is supported by the National Science Foundation through NSF/DMR-1644779 and the state of Florida. K.S.B. is grateful for the support of grateful for the support of the Office of Naval Research under Award number N00014-20-1-2308.

Author contributions

X.W. and X.L. conceived the project. X.W., J.C., H.L. and Z.L. performed the optical spectroscopy experiment under the supervision of D.S., W.X. and X.L. J.C. and Q.T. synthesized the bulk NiPS₃ crystal. X.W., H.K. and Q.T. prepared and characterized the exfoliated samples. A.C., A.H., S.S. and L.L. performed theoretical calculations. X.W. and X.L. performed the analysis and interpretation of the data with the significant input from K.S.B., S.S. and L.L. X.W. and X.L. wrote the manuscript with contributions from all authors.

References

- 1. Huang, B. et al. Layer-dependent ferromagnetism in a van der Waals crystal down to the monolayer limit. *Nature* **546**, 270-273 (2017).
- 2. Gong, C. et al. Discovery of intrinsic ferromagnetism in two-dimensional van der Waals crystals. *Nature* **546**, 265-269 (2017).
- 3. Burch, K. S., Mandrus, D. & Park, J.-G. Magnetism in two-dimensional van der Waals materials. *Nature* **563**, 47-52 (2018).
- 4. Gong, C. & Zhang, X. Two-dimensional magnetic crystals and emergent heterostructure devices. *Science* **363**, eaav4450 (2019).
- 5. Huang, B. et al. Emergent phenomena and proximity effects in two-dimensional magnets and heterostructures. *Nat. Mater.* **19**, 1276-1289 (2020).
- 6. Kim, K. et al. Suppression of magnetic ordering in XXZ-type antiferromagnetic monolayer NiPS₃. *Nat. Commun.* **10**, 345 (2019).
- 7. Kim, S. Y. et al. Charge-Spin Correlation in van der Waals Antiferromagnet NiPS₃. *Phys. Rev. Lett.* **120**, 136402 (2018).
- 8. Kang, S. et al. Coherent many-body exciton in van der Waals antiferromagnet NiPS₃. *Nature* **583**, 785-789 (2020).

- 9. Wang, X. et al. Spin-induced linear polarization of photoluminescence in antiferromagnetic van der Waals crystals. *Nat. Mater.* **20**, 964-970 (2021).
- 10. Hwangbo, K. et al. Highly anisotropic excitons and multiple phonon bound states in a van der Waals antiferromagnetic insulator. *Nat. Nanotechnol.* **16**, 655-660 (2021).
- 11. Afanasiev, D. et al. Controlling the anisotropy of a van der Waals antiferromagnet with light. *Sci. Adv.* 7, eabf3096 (2021).
- 12. Belvin, C. A. et al. Exciton-driven antiferromagnetic metal in a correlated van der Waals insulator. *arXiv preprint* arXiv:2106.08355 (2021).
- 13. Sandilands, L. J. et al. Spin-orbit excitations and electronic structure of the putative Kitaev magnet α-RuCl₃. *Phys. Rev. B* **93**, 075144 (2016).
- 14. Seyler, K. L. et al. Ligand-field helical luminescence in a 2D ferromagnetic insulator. *Nat. Phys.* **14**, 277-281 (2018).
- 15. Lee, J.-H. et al. Multiple spin-orbit excitons in α-RuCl3 from bulk to atomically thin layers. *npj Quantum Materials* **6**, 43 (2021).
- 16. Brink, J. v. d. & Sawatzky, G. A. Non-conventional screening of the Coulomb interaction in low-dimensional and finite-size systems. *Europhys. Lett.* **50**, 447-453 (2000).
- 17. Tan, P. H. et al. The shear mode of multilayer graphene. *Nat. Mater.* **11**, 294-300 (2012).
- 18. Lee, C. et al. Anomalous Lattice Vibrations of Single- and Few-Layer MoS₂. *ACS Nano* **4**, 2695-2700 (2010).
- 19. Wang, Y. et al. The range of non-Kitaev terms and fractional particles in α-RuCl3. npj Quantum Materials **5**, 14 (2020).
- 20. Wang, X. et al. Raman spectroscopy of atomically thin two-dimensional magnetic iron phosphorus trisulfide (FePS₃) crystals. *2D Mater.* **3**, 031009 (2016).
- 21. Lee, J.-U. et al. Ising-Type Magnetic Ordering in Atomically Thin FePS₃. *Nano Lett.* **16**, 7433-7438 (2016).
- 22. Yao, T., Mason, J. G., Huiwen, J., Cava, R. J. & Kenneth, S. B. Magneto-elastic coupling in a potential ferromagnetic 2D atomic crystal. *2D Mater.* **3**, 025035 (2016).

- 23. Liu, Z. et al. Observation of nonreciprocal magnetophonon effect in nonencapsulated few-layered CrI₃. *Sci. Adv.* **6**, eabc7628 (2020).
- 24. Huang, B. et al. Tuning inelastic light scattering via symmetry control in the two-dimensional magnet CrI3. *Nat. Nanotechnol.* **15**, 212-216 (2020).
- 25. Farhat, H. et al. Observation of Electronic Raman Scattering in Metallic Carbon Nanotubes. *Phys. Rev. Lett.* **107**, 157401 (2011).
- Fluegel, B., Mialitsin, A. V., Beaton, D. A., Reno, J. L. & Mascarenhas, A. Electronic Raman scattering as an ultra-sensitive probe of strain effects in semiconductors. *Nat. Commun.* 6, 7136 (2015).
- 27. Lane, C. & Zhu, J.-X. Thickness dependence of electronic structure and optical properties of a correlated van der Waals antiferromagnetic NiPS₃ thin film. *Phys. Rev. B* **102**, (2020).
- 28. Joy, P. A. & Vasudevan, S. Magnetism in the Layered Transition-Metal Thiophosphates MPS₃ (M = Mn, Fe, and Ni). *Phys. Rev. B* **46**, 5425-5433 (1992).
- 29. Wildes, A. R. et al. Magnetic structure of the quasi-two-dimensional antiferromagnet NiPS₃. *Phys. Rev. B* **92**, 224408 (2015).
- 30. Du, K. et al. Weak Van der Waals Stacking, Wide-Range Band Gap, and Raman Study on Ultrathin Layers of Metal Phosphorus Trichalcogenides. *ACS Nano* **10**, 1738-1743 (2016).
- 31. Devereaux, T. P. & Hackl, R. Inelastic light scattering from correlated electrons. *Rev. Mod. Phys.* **79**, 175-233 (2007).
- 32. Kuo, C.-T. et al. Exfoliation and Raman Spectroscopic Fingerprint of Few-Layer NiPS₃ Van der Waals Crystals. *Sci. Rep.* **6**, 20904 (2016).
- 33. Scagliotti, M., Jouanne, M., Balkanski, M., Ouvrard, G. & Benedek, G. Raman-Scattering in Antiferromagnetic FePS₃ and FePSe₃ Crystals. *Phys. Rev. B* **35**, 7097-7104 (1987).
- 34. Kuo, C.-T. et al. The energy band alignment at the interface between mechanically exfoliated few-layer NiPS3 nanosheets and ZnO. *Current Applied Physics* **16**, 404-408 (2016).

- Piacentini, M., Khumalo, F. S., Olson, C. G., Anderegg, J. W. & Lynch, D. W. Optical transitions, XPS, electronic states in NiPS₃. *Chem. Phys.* 65, 289-304 (1982).
- 36. Abramchuk, M. et al. Controlling Magnetic and Optical Properties of the van der Waals Crystal CrCl3-xBrx via Mixed Halide Chemistry. *Adv. Mater.* **30**, 1801325 (2018).
- 37. Wu, M., Li, Z., Cao, T. & Louie, S. G. Physical origin of giant excitonic and magneto-optical responses in two-dimensional ferromagnetic insulators. *Nat. Commun.* **10**, 2371 (2019).
- 38. Kotliar, G. et al. Electronic structure calculations with dynamical mean-field theory. *Rev. Mod. Phys.* **78**, 865-951 (2006).
- 39. Park, H., Millis, A. J. & Marianetti, C. A. Computing total energies in complex materials using charge self-consistent DFT + DMFT. *Phys. Rev. B* **90**, 235103 (2014).
- 40. Liu, R. et al. Novel Raman-active electronic excitations near the charge-transfer gap in insulating cuprates. *Phys. Rev. Lett.* **71**, 3709-3712 (1993).
- 41. Sanjuan, M. L., Kanehisa, M. A. & Jouanne, M. Electronic Raman Study of Fe²⁺ in FePX₃ (X=S,Se) Layered Compounds. *Phys. Rev. B* **46**, 11501-11506 (1992).
- 42. Ferraro, J. R., Nakamoto, K. & Brown, C. W., *Introductory Raman Spectroscopy*. (Elsevier, New York, 2003), vol. 1.
- 43. Ho, C.-H., Hsu, T.-Y. & Muhimmah, L. C. The band-edge excitons observed in few-layer NiPS3. *NPJ 2D Mater. Appl.* **5**, 8 (2021).
- 44. Cadiz, F. et al. Excitonic Linewidth Approaching the Homogeneous Limit in MoS₂-Based van der Waals Heterostructures. *Phys. Rev. X* **7**, 021026 (2017).
- 45. Basnet, R., Wegner, A., Pandey, K., Storment, S. & Hu, J. Highly sensitive spinflop transition in antiferromagnetic van der Waals material MPS₃ (M=Ni and Mn). *Physical Review Materials* **5**, 064413 (2021).
- 46. Ferre, J. & Gehring, G. A. Linear optical birefringence of magnetic crystals. *Rep. Prog. Phys* **47**, 513-611 (1984).

- 47. Bramwell, S. T. & Holdsworth, P. C. W. Magnetization and universal sub-critical behaviour in two-dimensional XY magnets. *J. Phys. Condens. Matter.* **5**, L53-L59 (1993).
- 48. Kresse, G. & Furthmüller, J. Efficiency of ab-initio total energy calculations for metals and semiconductors using a plane-wave basis set. *Comput. Mater. Sci.* **6**, 15-50 (1996).
- 49. Perdew, J. P., Burke, K. & Ernzerhof, M. Generalized Gradient Approximation Made Simple. *Phys. Rev. Lett.* **77**, 3865-3868 (1996).
- 50. Dudarev, S. L., Botton, G. A., Savrasov, S. Y., Humphreys, C. J. & Sutton, A. P. Electron-energy-loss spectra and the structural stability of nickel oxide: An LSDA+U study. *Phys. Rev. B* **57**, 1505-1509 (1998).
- 51. Grimme, S., Antony, J., Ehrlich, S. & Krieg, H. A consistent and accurate ab initio parametrization of density functional dispersion correction (DFT-D) for the 94 elements H-Pu. *J. Chem. Phys.* **132**, 154104 (2010).

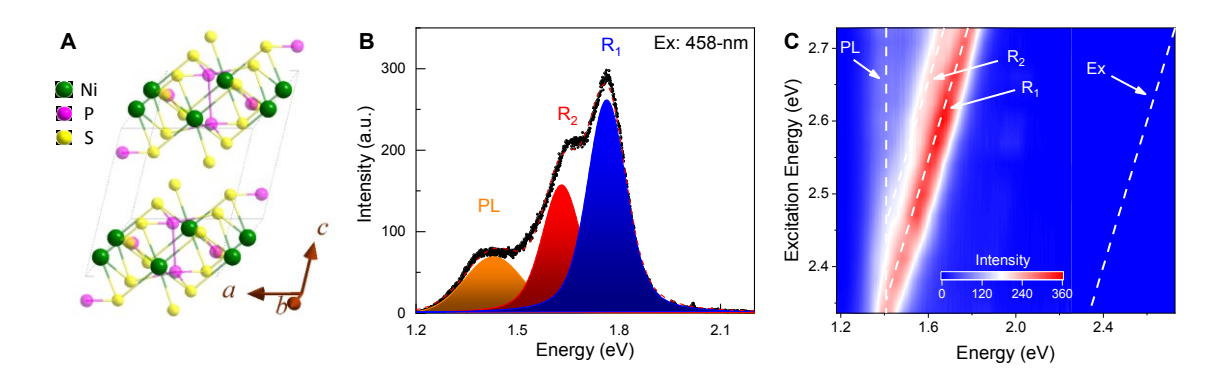


Fig. 1. Electronic Raman (ER) spectra of van der Waals (vdW) antiferromagnet NiPS₃. (A) Monoclinic crystal structure of NiPS₃. (B) Optical spectrum of bulk NiPS₃ excited by a 458-nm laser at 295 K. (C) Excitation-dependent photoluminescence (PL) and ER map of NiPS₃.

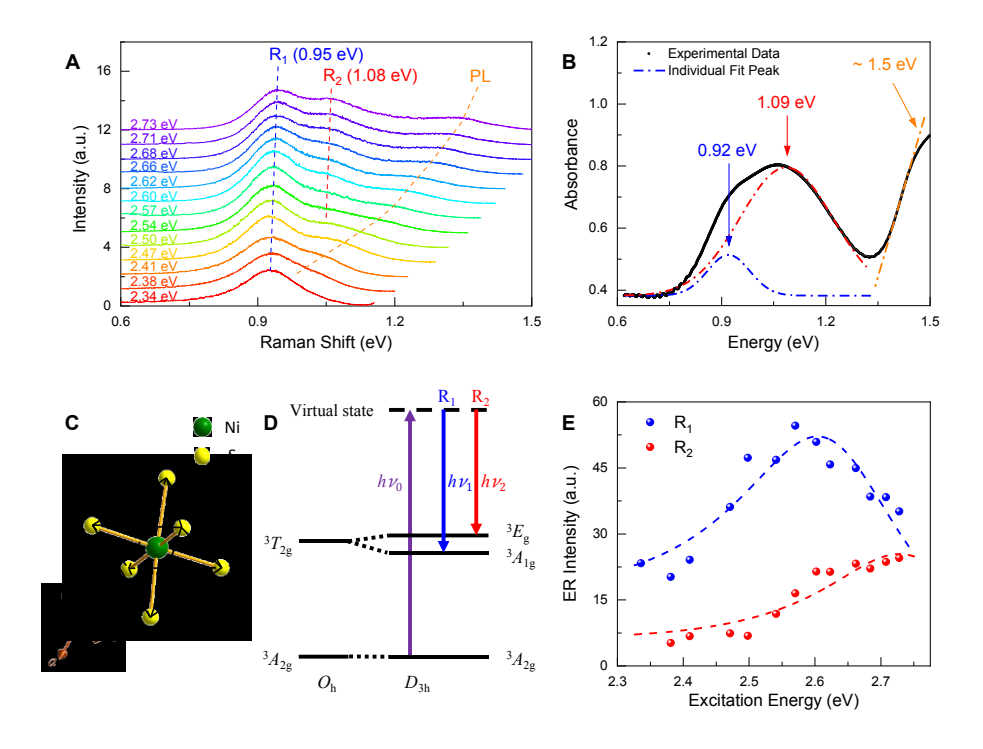


Fig. 2. Mechanism of electronic Raman (ER) modes in NiPS₃. (A) Optical spectra of NiPS₃ plotted in terms of Raman shift, *i.e.*, energy difference from excitation energy, excited by different lasers with energies from 2.73 to 2.34 eV. (B) Absorption spectrum of bulk NiPS₃ below the main absorption edge (\sim 1.5 eV), indicating a weak absorption feature consisting of two components. (C) Centered Ni²⁺ ion in a trigonally distorted octahedral sulfide environment. (D) Schematic illustration of ER scattering in between the ground state and first excited triplet state for Ni²⁺ ion in a trigonally distorted octahedral environment (D_{3h}). O_h represents the crystal field splitting in an octahedral field; hv_0 and $hv_1(hv_2)$ are the energy of incident and scattered photons of R₁ (R₂) mode. (E) Integrated intensity of two ER peaks as a function of excitation energy. The dashed lines are the fitting curves.

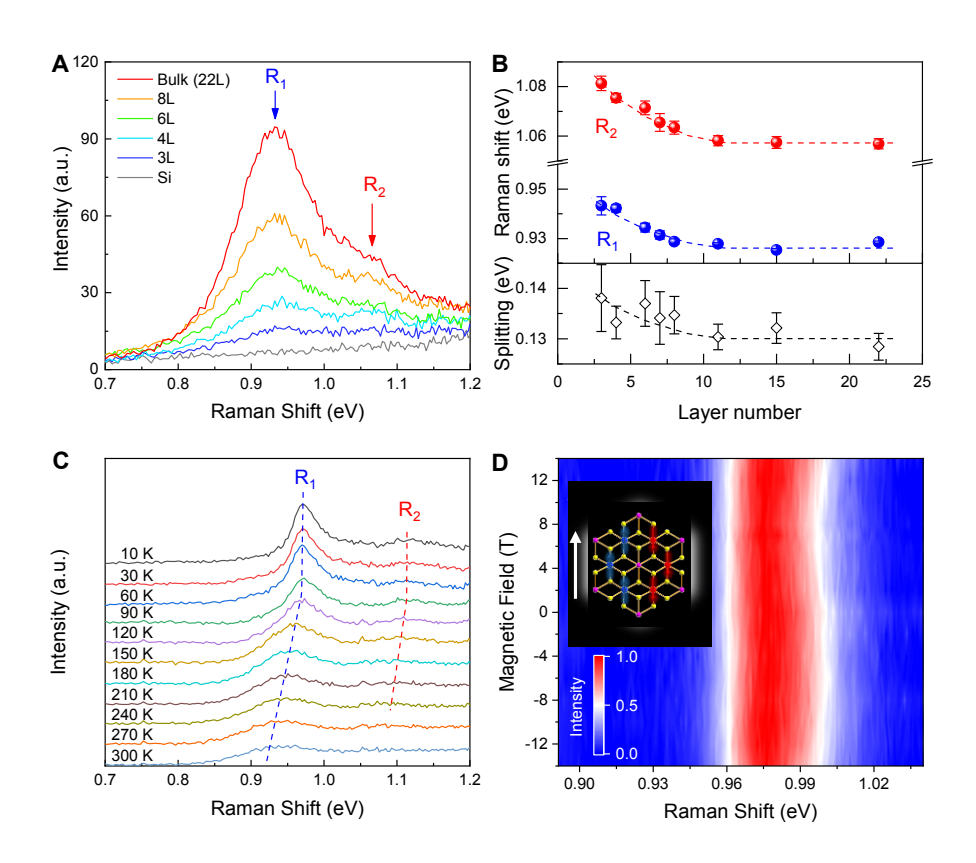


Fig. 3. Localized nature and magnetic robustness of ER modes. (A) Thickness-dependent ER spectra of NiPS₃ from bulk down to 3-layer. (B) Raman shift of two ER peaks and the energy splitting as a function of sample thickness. The evolution trends of R₁, R₂ and energy splitting are guided by the blue, red and black dashed lines, respectively. (C) Temperature-dependent ER spectra excited by 458-nm laser from 10 to 300 K. (D) Color map of magnetic-field-dependent ER spectra with in-plane field along *a*-axis (B_{||}) under 488-nm laser excitation. The inset represents the direction of applied magnetic field with respect to the antiferromagnetic spin structure of NiPS₃.

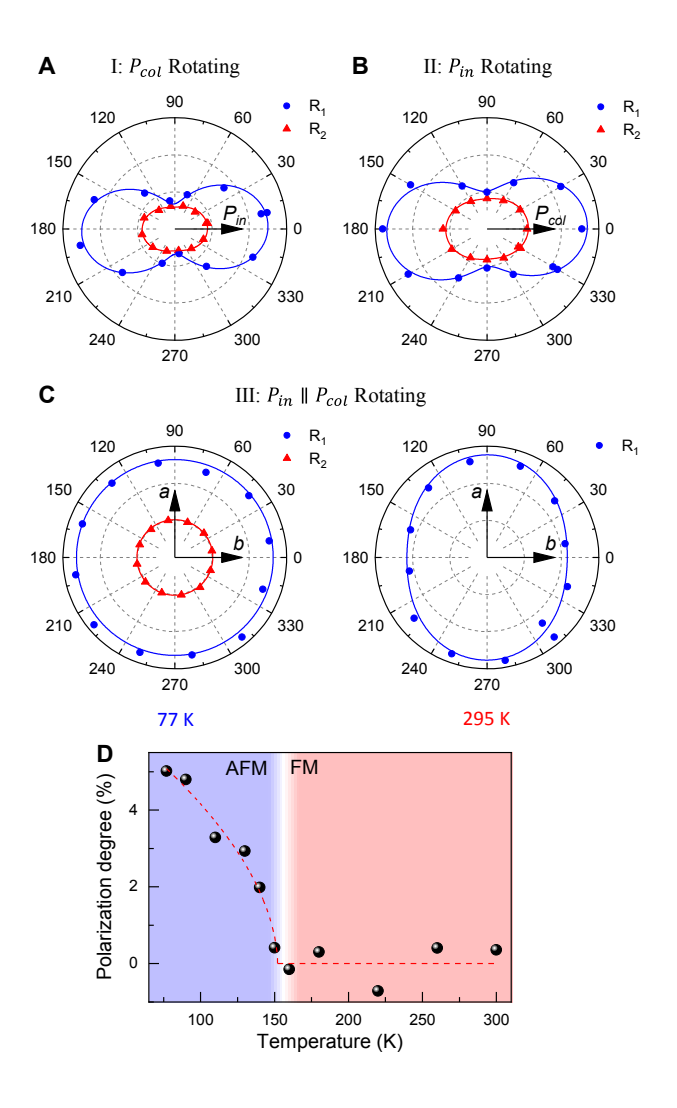


Fig. 4. Polarization-resolved ER modes in the layered antiferromagnetic NiPS₃. (A) Polar plot of ER intensity of NiPS₃ as a function of P_{col} angle excited by 473-nm laser with fixed P_{in} (Configurations I) at 295 K. (B) Polar plot of ER intensity of NiPS₃ as a function of P_{in} angle excited by 473-nm laser with fixed P_{col} (Configurations II) at 295 K. (C) Polar plot of ER intensity of NiPS₃ as a function azimuthal angle excited by a 473-nm laser with $P_{in} \parallel P_{col}$ (Configurations III) at 295 and 77 K. The a and b axis of crystal were labelled in (C). (D) Polarization degree of ER₁ as a function of temperature. The red dashed line is the fitting using the formula, $\rho(T) \sim \left|1 - \frac{T}{T_N}\right|^{2\beta}$, where $\beta = 0.27 \pm 0.03$.